

# Ultraviolet Resonance Raman Studies Reveal the Environment of Tryptophan and Tyrosine Residues in the Native and Partially Folded States of the E Colicin-Binding Immunity Protein Im7<sup>†</sup>

Iñigo R. Rodriguez-Mendieta,<sup>‡,§</sup> Graham R. Spence,<sup>‡,||</sup> Christopher Gell,<sup>‡,§</sup> Sheena E. Radford,<sup>‡,||</sup> and D. Alastair Smith<sup>\*,‡,§</sup>

*Institute of Molecular Biophysics and Astbury Centre for Structural Molecular Biology, School of Physics and Astronomy, and School of Biochemistry and Microbiology, University of Leeds, Leeds LS2 9JT, United Kingdom*

*Received October 21, 2004; Revised Manuscript Received December 22, 2004*

**ABSTRACT:** Understanding the nature of partially folded proteins is a challenging task that is best accomplished when several techniques are applied in combination. Here we present ultraviolet resonance Raman (UVRR) spectroscopy studies of the E colicin-binding immunity proteins, Im7\* and Im9\*, together with a series of variants of Im7\* that are designed to trap a partially folded state at equilibrium. We show that the environments of the tryptophan and tyrosine residues in native wild-type Im7\* and Im9\* are indistinguishable, in contrast with models for their structures based on X-ray and NMR methods. In addition, we show that there is a general increase in the hydrophobicity in the environment of Trp75 in all of the variants compared with wild-type Im7\*. These data suggest that a significant rearrangement of the tryptophan pocket occurs in the variants, which, together with an overall decrease in solvent accessibility of Trp75 as judged by time-resolved fluorescence lifetime measurements and fluorescence quenching experiments, rationalize the unusual fluorescence properties of the variants reported previously. The data highlight the power of UVRR in analyzing the structural properties of different conformational states of the same protein and reveal new information about the structural rearrangements occurring during Im7\* folding, not possible using other spectroscopic methods alone. Finally, we describe a previously unreported dependence of the tryptophan Fermi doublet on excitation wavelength in the ultraviolet region revealed by these protein spectra. We corroborated this observation using tryptophan-containing model compounds and conclude that the conventional interpretation of this UVRR feature at these wavelengths is unreliable.

The biological role of the E colicin-binding immunity proteins Im2, Im7, Im8, and Im9 is to protect the host cell from the toxic endonuclease activity of a coexpressed cognate colicin, by binding to an exosite in the DNase domain, inhibiting access of the substrate DNA to the active site of the colicin by steric hindrance and electrostatic repulsion (1, 2). The small size of the immunity proteins (85–87 amino acid residues), their high level of sequence identity (approximately 60%), the single conserved tryptophan, and their lack of disulfide bonds, prosthetic groups, and *cis*-prolines in the native state make the immunity protein family ideal for protein folding studies. Despite the high degree of similarity between Im7 and Im9 in both sequence and structure, these proteins fold by mechanisms with different levels of kinetic complexity at neutral pH, suggesting that

local sequence variations, rather than topology or global stability, are responsible for the observed folding kinetics of these proteins (3–7). Im7\*<sup>1</sup> and Im9\* (hexahistidine-tagged analogues of Im7 and Im9) contain four helices (Figure 1A), each of which displays polar side chains on the surface of the protein, while the majority of hydrophobic side chains are buried, forming a well-packed hydrophobic core. Im7\* and Im9\* share very similar distorted four-helix bundle structures, although the loop between helices I and II is one residue shorter in Im9\* than in Im7\*, resulting in small but functionally important differences in the manner in which the four helices pack. Helix III is the shortest helix in the immunity proteins, being only six residues long. Nonetheless, the sequence of this helix is one of the most highly conserved regions of the protein (1, 2), being largely invariant in all four immunity family members (the sequence of this helix is Thr51-Asp52-Leu53-Ile54-Tyr55-Tyr56 in

<sup>†</sup> We acknowledge the Biology and Biotechnology Research Council (Grant 24/E16849), The Wellcome Trust, and the University of Leeds for financial support. S.E.R. is a BBSRC Professorial Fellow.

\* To whom correspondence should be addressed: School of Physics and Astronomy, University of Leeds, Leeds LS2 9JT, United Kingdom. Telephone: +(44) 113 343 3875. Fax: +(44) 113 343 1885. E-mail: d.a.m.smith@leeds.ac.uk.

<sup>‡</sup> Institute of Molecular Biophysics and Astbury Centre for Structural Molecular Biology.

<sup>§</sup> School of Physics and Astronomy.

<sup>||</sup> School of Biochemistry and Microbiology.

<sup>1</sup> Abbreviations: AcTrpEE, *N*-acetyl-L-tryptophan ethyl ester; Ac-TrpMA, *N*-acetyltryptophan methylamide; CSU, Contacts of Structural Units; fwhm, full width at half-maximum; Im7\*, hexahistidine-tagged Im7; Im9\*, hexahistidine-tagged Im9;  $k_q$ , quenching constant;  $K_{sv}$ , Stern–Volmer constant;  $\lambda_{max}$ , maximum emission wavelength; NATA, *N*-acetyl-L-tryptophanamide; NMR, nuclear magnetic resonance; UV, ultraviolet; UV CD, ultraviolet circular dichroism; UVRR, ultraviolet resonance Raman.

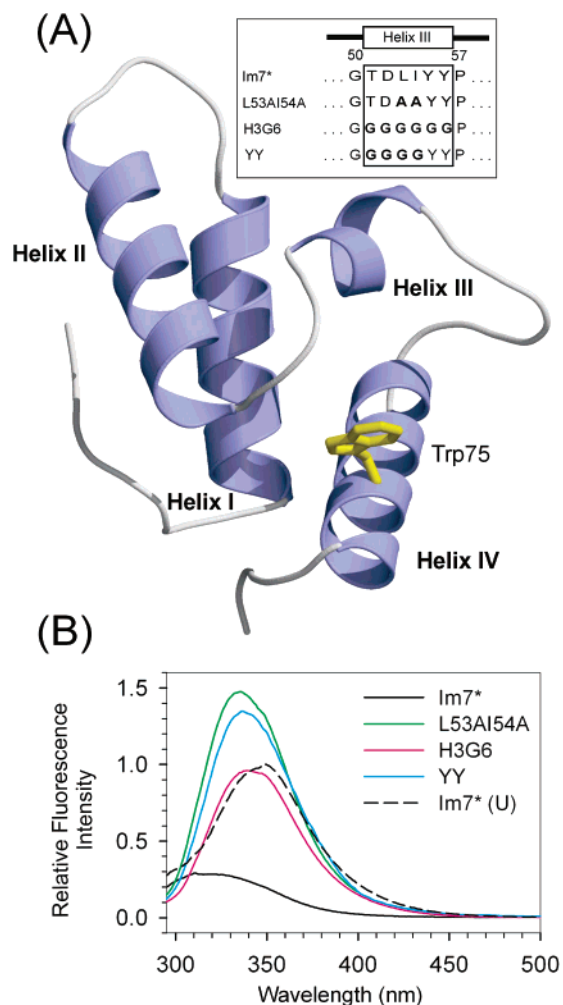


FIGURE 1: (A) Ribbon diagram of Im7 showing helices I–IV. The side chain of Trp75 is colored yellow. The mutations made to the sequence encompassing helix III in the Im7\* variants L53AI54A, H3G6, and YY are shown (inset). Panel A was drawn using Molscript (36) and Raster3D (37) from the coordinates of the crystal structure of Im7 (PDB entry 1AYI) (1). (B) Fluorescence emission spectra of the folded states of wild-type Im7\* (black), L53AI54A (green), H3G6 (pink), and YY (light blue) relative to the denatured states of each protein in 8 M urea, and the 8 M urea denatured state of wild-type Im7\* (dashed black).

Im7\*). This helix plays an important role in the interaction between the immunity proteins and their cognate colicins (8, 9), and is also essential for the folding of Im7 and Im9 to their native, functional states (6, 7).

The presence of a unique, conserved tryptophan residue (Trp75 in Im7\* and Trp74 in Im9\*) and three tyrosine residues (Tyr10, Tyr55, and Tyr56 in Im7\* and Tyr10, Tyr54, and Tyr55 in Im9\*) make these proteins suitable for study by ultraviolet resonance Raman (UVRR) spectroscopy. Using 229 nm excitation (10), the tryptophan and tyrosine Raman bands are selectively enhanced (11, 12), enabling UVRR spectroscopy to provide structural and environmental information concerning the side chains of these aromatic residues. Here, we report UVRR studies of the native structures of Im7\* and Im9\*, together with three variants of Im7\* [termed L53AI54A, H3G6, and YY (inset of Figure 1A)], that trap a partially folded state of Im7\* at equilibrium by preventing the binding of helix III to the developing structure (13). These mutations selectively destabilize native Im7\* such that the on-pathway folding intermediate becomes

the ground state of folding in the absence of a denaturant. In the Im7\* variant L53AI54A, residues Leu53 and Ile54 in helix III, which are buried in the core of the native structure, are replaced with alanine residues. In H3G6, all six residues that comprise the native helix III are replaced with glycine residues. Finally, in the variant YY, residues Thr51–Ile54 in helix III have been substituted with glycine, leaving wild-type residues Tyr55 and Tyr56 in the native helix III intact (inset of Figure 1A). Interestingly, the variants YY and L53AI54A have very similar near- and far-UV circular dichroism (UV CD) spectra, stabilities, *m*-values (G. R. Spence and S. E. Radford, unpublished results), and fluorescence emission spectra (Figure 1B). All of these variants have been shown to fold to a partially folded state at equilibrium that resembles the kinetic folding intermediate of wild-type Im7\* in many spectroscopic and thermodynamic properties (13; G. R. Spence and S. E. Radford, unpublished results). Interestingly, however, the fluorescence intensity of Trp75 in these variants differs (Figure 1B). Thus, while the fluorescence intensity of Trp75 in the folded states of L53AI54A and YY is hyperfluorescent (being greater than that of their respective unfolded states), akin to the properties of the kinetic folding intermediate of wild-type Im7\* (4–6), the folded and unfolded states of the variant H3G6 (Figure 1B) have equal intensity (13). A major unresolved question about these proteins, therefore, is the origin of their hyperfluorescence and the nature of the side chain interactions responsible for tailoring the fluorescence of Trp75 in these species. Here we have used UVRR spectroscopy to probe the structural differences between the native states of wild-type Im7\* and Im9\*, together with the folded states of the variants, L53AI54A, H3G6, and YY. The data demonstrate the power of UVRR spectroscopy to identify and characterize subtle differences in the conformational properties of closely related structures and provide new insights into the structural variability in different conformational states of the same protein. In addition, by careful analysis of the response of the tryptophan Fermi doublet to the excitation wavelength in a series of model compounds and in the immunity proteins, we have found that the accepted interpretation of this UVRR feature for excitation at 229 nm is not reliable.

## MATERIALS AND METHODS

**Immunity Protein Preparation.** Im7\*, Im9\*, and the Im7\* variants L53AI54A, H3G6, and YY were expressed and purified as previously described (7, 13). All residues are numbered according to the sequence of the untagged proteins. To allow correct normalization of the UVRR spectra, the extinction coefficient of the folded state at 280 nm of each protein determined as described in ref 13, based on the method of Gill and von Hippel (14), was used to ensure that all protein concentrations were 150  $\mu$ M. All UVRR spectra of the immunity proteins were acquired at 10 °C in 50 mM sodium phosphate buffer (pH 7.0) containing 1 mM EDTA and 0.4 M sodium sulfate. The latter salt was included since it has been shown to stabilize the kinetic intermediate as well as the trapped intermediate species at equilibrium (4, 13).

**UVRR Spectroscopy.** UVRR spectra were obtained with a Renishaw Raman System 1000 spectrometer described elsewhere (15), adapted for use at 229 and 244 nm using approximately 0.3 mW at the sample generated by an

Table 1: Visible and UV Raman Tryptophan Fermi Doublet Ratios ( $R = I_{1360}/I_{1340}$ ) for Model Compounds in Different Solvents

	633 nm <sup>a</sup>	488 nm <sup>a</sup>	244 nm <sup>a</sup>	229 nm <sup>a</sup>	488 nm <sup>a</sup> (24)
indole in acetonitrile	0.69	0.67	0.52	0.57	0.71
indole in methanol	0.92	0.78	0.55	0.735	0.92
AcTrpEE in acetonitrile	1.01	1.00	0.813	1.53	1.06
AcTrpEE in methanol	1.11	1.04	0.92	1.36	1.26
NATA in H <sub>2</sub> O	—	—	0.75	1.11	—

<sup>a</sup> Excitation wavelengths.Table 2: Position of the Y8b/Y8a Modes for Im7\* and the Three Im7\* Variants<sup>a</sup>

	position (cm <sup>-1</sup> )	
	Y8b	Y8a
Im7*	1599.2 ± 0.5	1615.0 ± 0.2
L53AI54A	1600.7 ± 0.6	1616.1 ± 0.15
H3G6	1601.8 ± 0.6	1616.2 ± 0.19
YY	1601.9 ± 0.7	1616.2 ± 0.2

<sup>a</sup> Experimental frequencies obtained by curve fitting the 1510–1680 cm<sup>-1</sup> region with 50% Gaussian and 50% Lorentzian bands (see the Supporting Information).

intracavity frequency-doubled argon ion laser (Coherent Innova 300 FreD). A peristaltic pump was used to circulate the protein samples from a thermostated reservoir through a 0.2 mm inner diameter quartz capillary tube held in a thermostated block. UVR spectra were acquired at 10 °C in 5 min (60 s per five accumulations). Protein concentrations were 150 μM, at which all of these proteins are monomeric, as measured by analytical ultracentrifugation and analysis of the protein concentration dependence of the refolding kinetics (13, 16). Spectral intensities were normalized, after baseline correction, using the band arising from sulfate at 981 cm<sup>-1</sup>. The capillary was washed between measurements using a buffer solution, and wild-type Im7\* control spectra were established between each measurement. The integrity of the samples under UV light was confirmed separately by subtracting the spectra obtained after 1, 10, and 30 min, giving a flat line in all cases after intensity normalization. Fitting of the W3 and Y8a/Y8b Raman bands was achieved using a 50% Gaussian and 50% Lorentzian distribution using the GRAMS 32 CurveFit routine (Galactic Industries Corp.). One band at ~1650 cm<sup>-1</sup>, due to the amide I mode and water contribution, was included during the fitting process. The quality of the fit was evaluated by comparing the  $\chi^2$  values and the residuals of the fit. Curve fitting results are shown in the Supporting Information, and peak positions are summarized in Table 2. The tryptophan derivatives *N*-acetyl-L-tryptophanamide (NATA) in water and *N*-acetyl-L-tryptophan ethyl ester (AcTrpEE) and indole (Sigma Chemicals) in methanol or acetonitrile were used at concentrations of 1 and 5 mM, respectively. Spectra of the solvents were collected separately, and their contributions were subtracted from the relevant spectrum of each model compound.

**Fluorescence Emission Spectra.** Fluorescence emission spectra of wild-type Im7\* and the variants L53AI54A, H3G6, and YY were measured using a Photon Technology International fluorimeter (Ford, West Sussex, U.K.). For spectra of native and denatured states, each protein was dissolved in 50 mM sodium phosphate buffer (pH 7.0) containing 0.4 M sodium sulfate and 1 mM EDTA or the same buffer containing 8 M urea, respectively, at a known protein

concentration of approximately 20 μM. The excitation wavelength was 280 nm, and excitation and emission slits were set to 2 and 3 nm, respectively. Each spectrum was acquired from 270 to 450 nm in 1 nm increments, integrating for 1 s at each wavelength. The fluorescence intensity of the denatured states was assumed to be equal at 350 nm. Spectra of the folded state of each protein in the absence of urea were then normalized to the intensity of their respective denatured states. In this manner, a direct comparison of the fluorescence intensity of the variants with that of kinetic intermediate can be made.

**Fluorescence Lifetime Measurements.** Fluorescence lifetimes for the wild-type proteins and variants in 50 mM sodium phosphate buffer (pH 7.0) containing 1 mM EDTA and 0.4 M sodium sulfate were obtained at 10 °C. Measurements were made using the time-correlated single photon counting technique with an Edinburgh Instruments FL900DCT fluorescence spectrometer incorporating a Hamamatsu R3809 microchannel plate photomultiplier tube. The excitation source was a cavity-dumped dye laser, synchronously pumped by a frequency-doubled mode-locked Nd:YAG laser. The cavity-dumped output from the dye laser was frequency-doubled to produce an excitation source at 295 nm with a pulse width of approximately 8 ps. Emission was detected at 350 nm for all of the proteins. The instrument response function had a full width at half-maximum of 50 ps. The fluorescence decays,  $I(t)$ , were measured with the emission polarizer at the “magic angle” and were fitted by iterative reconvolution of the instrument function with a sum of exponentials of the form

$$I(t) = \sum_{i=1}^n \alpha_i \exp(-t/\tau_i) \quad (1)$$

where  $\alpha_i$  values are the amplitudes of the exponential function decay constants  $\tau_i$ . The number of exponentials used,  $n$ , was the minimum required to achieve a good fit, which was assessed by examination of the residuals and the calculated  $\chi^2$  value. Weighted average lifetimes were calculated on the basis of the mean lifetime of a multiexponential decay, given by

$$\bar{\tau} = \sum_{i=1}^n f_i \tau_i \quad (2)$$

where  $f_i$  is the fractional intensity corresponding to the lifetime component  $\tau_i$  and  $\alpha_i$  is the pre-exponential factor

$$f_i = \frac{\alpha_i \tau_i}{\sum_j \alpha_j \tau_j} \quad (3)$$

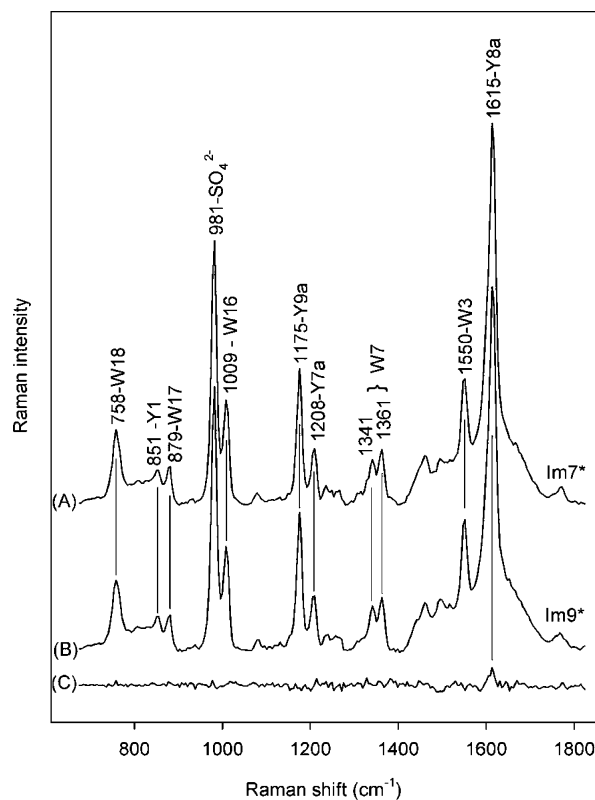


FIGURE 2: 229 nm excited UVRR spectra of Im7\* (A) and Im9\* (B) and the Im7\* minus Im9\* difference spectrum (C). Spectra were acquired in 5 min and normalized using the sulfate band at  $981\text{ cm}^{-1}$  after baseline correction. The protein concentration was adjusted to  $150\text{ }\mu\text{M}$  using the corresponding extinction coefficient determined at  $280\text{ nm}$  for each protein (13).

Errors in mean lifetimes were determined from the uncertainties in the individual lifetimes obtained in the fitting process.

## RESULTS

*A Comparison of the Solution Structures of Im7\* and Im9\* by UVRR.* The structures of Im7 (1) and Im9 (17) have been determined by X-ray crystallography and NMR, respectively. Both proteins fold rapidly to their native states in which fixed and specific interactions involving the aromatic side chains of the single tryptophan (Trp75 in Im7\* and Trp74 in Im9\*) and three tyrosine residues (Tyr10, Tyr55, and Tyr56 in Im7\* and Tyr10, Tyr54, and Tyr55 in Im9\*) occur. Figure 2 shows the UVRR spectra excited at  $229\text{ nm}$  of Im7\* and Im9\* and their difference spectrum. At this excitation wavelength, strong enhancement is observed for the Raman bands arising from tryptophan and tyrosine residues in resonance through their  $B_b$  and  $L_a$  electronic transitions, respectively (18–21). Tryptophan bands are observed at  $1550$  (W3),  $1361$ – $1341$  (W7),  $1009$  (W16),  $879$  (W17), and  $758\text{ cm}^{-1}$  (W18). Tyrosine band positions are  $1615$  (Y8a),  $1599$  (Y8b),  $1208$  (Y7a),  $1175$  (Y9a), and  $851\text{ cm}^{-1}$  (Y1).

The frequency of the W17 band is known to be sensitive to the strength of hydrogen bonding at the indole nitrogen of tryptophan residues (22). This band is present in Im7\* and Im9\* at an identical wavenumber of  $879\text{ cm}^{-1}$ , a position that correlates with moderate to weak hydrogen bonding (22) of the indole nitrogen of Trp75/74, respectively, in these proteins. Analysis of the crystal and solution structures of

Im7 and Im9 suggests that the single tryptophan residue in these proteins does not hydrogen bond to other residues in the structure. Thus, the position of the W17 band, combined with the structural data, suggests that the single tryptophan residue in each protein forms hydrogen bonds with water. In accord with this, the indole ring of tryptophan in both proteins is at least partially exposed to solvent in their crystal or solution structures with solvent accessible surface areas of  $\sim 105$  and  $\sim 40\text{ }\text{\AA}^2$  for Trp75/74 in Im7 and Im9, respectively, as determined by CSU (Contacts of Structural Units) (23). The intensity of the tryptophan bands in UVRR spectra can be used to assess the hydrophobicity of the environment surrounding tryptophan residues. Interestingly, the intensity of these bands is identical in the UVRR spectra of Im7\* and Im9\* (Figure 2A,B), resulting in a featureless difference spectrum (Figure 2C), and indicating that the overall hydrophobicity of the environment surrounding the tryptophan residue is identical in the two proteins. Thus, the differences in solvent accessible surface area of the indole ring of the single tryptophan residue in Im7\* and Im9\* suggested by the structural models for these proteins must be compensated by local differences in the environment of the tryptophan pocket. (In the native structures of the two proteins, 10 residues contact Trp75/74, of which only three are different in the primary sequence of the two proteins: Glu71, Ile72, and Glu74 in Im7 are substituted with Thr70, Val71, and Asn73, respectively, in Im9.) Alternatively, the apparent differences in solvent exposure of the indole ring of Trp75/74 in the two proteins estimated by comparison of their crystal (for Im7) and solution (for Im9) structures may simply not occur for the proteins in solution. Whatever the structural origins of this effect, however, the UVRR data demonstrate unequivocally that the overall hydrophobicity of the environment of Trp75/74 in these homologous proteins is identical.

The intensity ratio of the tryptophan Fermi doublet at  $1360/1340\text{ cm}^{-1}$  can also be used as an indicator of the overall hydrophobicity of the environment surrounding tryptophan residues (24). The tryptophan doublet arises from a Fermi resonance between a fundamental mode at  $\sim 1340\text{ cm}^{-1}$  and a combination of two out-of-plane modes involving the benzene and pyrrole rings comprising the tryptophan side chain (25). The Fermi doublet is identical for Im7\* and Im9\* (Figure 2A,B), resulting in no feature in the difference spectrum (Figure 2C), consistent with Trp75/74 occupying identical environments in these proteins. However, the intensity ratio,  $R (=I_{1360}/I_{1340})$ , is greater than unity for both proteins ( $R_{\text{Im7}^*}^{229} = 1.16$  and  $R_{\text{Im9}^*}^{229} = 1.14$ ). According to the accepted interpretation of this doublet (24), a ratio greater than unity suggests a net hydrophobic environment of the indole ring, in direct disagreement with the interpretation of the position of the W17 band and the X-ray and NMR structures of the two native proteins (1, 17). This disagreement (and similar anomalous data for the Fermi doublet of the variants presented and discussed below) prompted us to investigate the behavior of the tryptophan Fermi doublet using the model compounds *N*-acetyl-L-tryptophanamide (NATA), *N*-acetyl-L-tryptophan ethyl ester (AcTrpEE), and indole. The visible and UV Raman spectra of these compounds were obtained at  $633$ ,  $488$ ,  $244$ , and  $229\text{ nm}$  in water, methanol, and acetonitrile. The  $I_{1360}/I_{1340}$  ratios are sum-



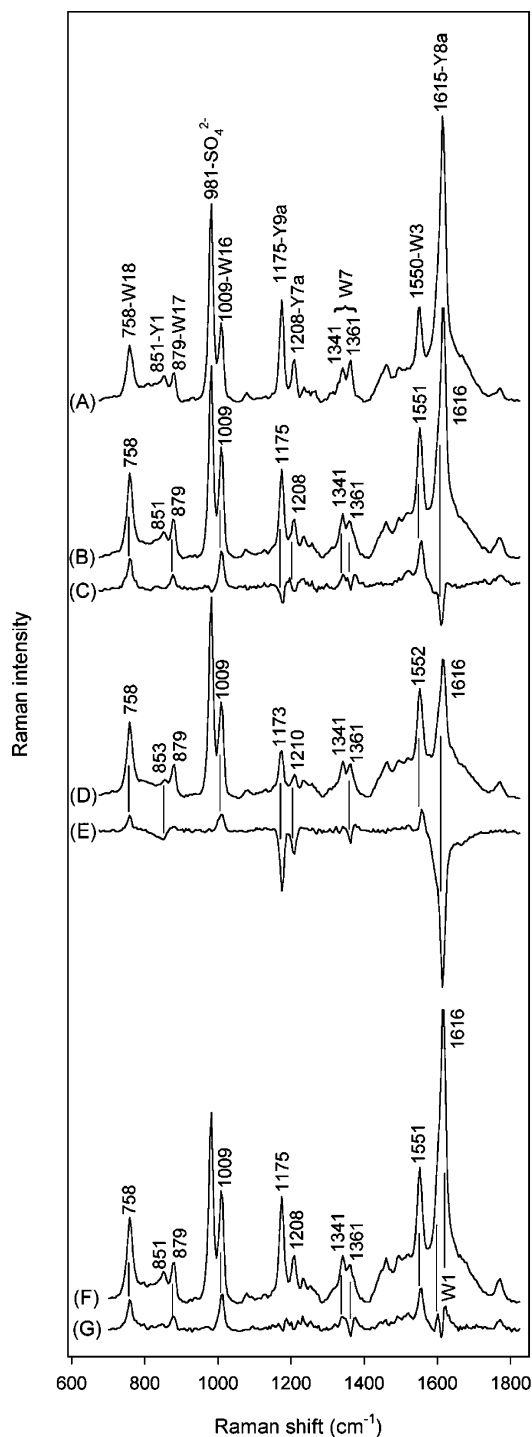


FIGURE 5: 229 nm excited UVRR spectra of Im7\* (A) and L53AI54A (B) and the L53AI54A minus Im7\* difference spectrum (C), H3G6 and the H3G6 minus Im7\* difference spectrum (D and E, respectively), and YY and the YY minus Im7\* difference spectrum (F and G, respectively). Spectra were acquired in 5 min and normalized using the sulfate band at 981  $\text{cm}^{-1}$  after baseline correction. The protein concentration was adjusted to 150  $\mu\text{M}$  using the corresponding extinction coefficient determined at 280 nm for each protein.

The W3 position in Im7\* and Im9\* is at 1550  $\text{cm}^{-1}$  [full width at half-maximum (fwhm) = 14.5  $\text{cm}^{-1}$ ] and correlates with a  $|\chi^{2,1}|$  angle of  $94 \pm 3^\circ$ , according to the relationship given by Maruyama and Takeuchi (28). The correlation between the W3 band position and  $|\chi^{2,1}|$  is not capable of distinguishing between opposite ring orientations due to the

plane of symmetry of the indole ring along the  $C_\alpha$  atom. Given this caveat, the UVRR data in Figure 2 show identical magnitudes for this dihedral angle in Im7\* and Im9\*. However, X-ray diffraction data show that Trp75 in Im7 has a  $\chi^{2,1}$  value of  $-101^\circ$ , whereas NMR studies of Im9 show an average  $\chi^{2,1}$  value of  $69^\circ$ . The origin of the differences in the properties of Trp75/74 in these proteins according to X-ray crystal and NMR solution structures is not clear. One influencing factor may be the differences in experimental conditions between the crystalline form of Im7 and solution forms of Im9 (NMR experiments carried out with the same pH and buffer conditions used here for the UVRR study, except that the buffer lacked 0.4 M sodium sulfate and the protein concentration was approximately 1 order of magnitude greater in NMR experiments). In addition, the temperature at which the measurements were taken varied between the UVRR (10  $^\circ\text{C}$ ) and NMR and X-ray experiments (20  $^\circ\text{C}$ ). Nonetheless, this again demonstrates the power of UVRR difference spectroscopy to provide a simple comparative probe in solution of a single tryptophan in a protein under identical conditions.

UVRR bands Y7a, Y8a, and Y9a (Figure 2A,B) arise from the three tyrosine residues present in Im7\* and Im9\*. The position and intensity of these bands are known to be sensitive indicators of hydrogen bonding and hydrophobicity, respectively, in the local environment of the tyrosine residues (29–32). The positions of all three tyrosine bands in Im7\* and Im9\* are identical. Tyrosine bands Y8b and Y8a are present at 1599 and 1615  $\text{cm}^{-1}$ , positions that correlate with that observed for tyrosine in an aqueous solvent (29). A weak positive signal is present in the difference spectrum at the Y8a position (1613  $\text{cm}^{-1}$ ) with an intensity that is approximately 4% of the raw Y8a band intensity (Figure 2C). Given that the noise in these difference spectra is  $\sim 2\%$ , it is difficult to draw any clear conclusions about this small feature. Overall, the identical positions and intensities of the Raman bands arising from tyrosine residues suggest that the three tyrosine residues in Im7\* and Im9\* adopt identical conformations, in agreement with their solvent accessible surface areas and patterns of hydrogen bonding calculated from their X-ray and NMR structures (1, 17).

*UVRR Indicates that the Environment Local to Trp75 Is Non-Native in the Partially Folded Variants of Im7\*.* To study the conformational properties of the on-pathway folding intermediate of Im7\* in more detail and, in particular, the origins of the non-native interactions that stabilize this species (6) and give rise to its unusual and characteristic hyperfluorescence [the intermediate is more fluorescent than both the native and denatured states of wild-type Im7\* (4–6)], a series of Im7\* variants in each of which one or more residues in helix III was substituted with Ala or Gly was designed, expressed, and characterized (13). As a consequence, helix III can no longer bind to the developing hydrophobic core of Im7\*, effectively trapping a partially folded state at equilibrium. Three of these variants are studied here (L53AI54A, H3G6, and YY; Figure 1A, inset). In the variant L53AI54A, the two hydrophobic side chains of Leu53 and Ile54, known to stabilize the interactions between helix III and the rest of the hydrophobic core in native Im7\* (6), are substituted with alanine residues. As a consequence, the native state of Im7 is substantially destabilized, while the stability of the intermediate, in which helix III is not yet

Table 3: Fluorescence Lifetimes  $\tau$ , Stern–Volmer Constants  $K_{sv}$ , and Quenching Rate Constants  $k_q$  of Im7\* and the Variants L53AI54A, H3G6, and YY<sup>a</sup>

	$\tau_1$ (ns)	$\alpha_1$	$\tau_2$ (ns)	$\alpha_2$	$\tau_3$ (ns)	$\alpha_3$	$\tau_4$ (ns)	$\alpha_4$	$\bar{\tau}$ (ns) <sup>b</sup>	$K_{sv}$ (M <sup>-1</sup> ) <sup>c</sup>	$k_q$ ( $\times 10^9$ M <sup>-1</sup> s <sup>-1</sup> ) <sup>d</sup>
Im7*	0.154	0.119	1.452	0.032	5.610	0.006	0.440	0.097	1.98	1.5	0.757
L53AI54A	0.696	0.091	3.18	0.129	6.470	0.128	—	—	5.15	2.8	0.543
H3G6	0.147	0.083	0.869	0.118	3.205	0.148	7.190	0.072	4.81	4.0	0.830
YY	0.830	0.103	3.256	0.136	6.663	0.108	—	—	5.05	2.9	0.585

<sup>a</sup> Mean lifetimes  $\bar{\tau}$  were calculated using  $\bar{\tau} = \sum f_i \tau_i$ , where  $f_i$  is the fractional amplitude corresponding to the lifetime component  $\tau_i$ . <sup>b</sup> Errors in mean lifetimes estimated from the uncertainties in the individual lifetimes obtained from the fitting process are  $\pm 0.068$  for Im7\* and  $\pm 0.1$  for the rest of the variants. <sup>c</sup> Quoted  $K_{sv}$  values were obtained from iodide quenching experiments (13). <sup>d</sup> Errors in the calculated  $k_q$  values are  $\pm 0.027$  for Im7\*,  $\pm 0.022$  for L53AI54A and YY, and  $\pm 0.044$  for H3G6.

formed or docked against the developing core, is not affected by the substitutions. This results in the population of a hyperfluorescent partially folded species at equilibrium (Figure 1B) that closely resembles the kinetic intermediate species in many of its properties (13). In the variant H3G6, the six residues that comprise helix III in native Im7\* are substituted with (Gly)<sub>6</sub>, also preventing formation of the native state. This species resembles L53AI54A in terms of its secondary structure and thermodynamic stability, but is fascinating in that the single tryptophan residue in this species is not hyperfluorescent (Figure 1B) (13). The variant YY was constructed to examine the role of the side chains of residues Tyr55 and Tyr56 in helix III in tailoring the properties of the intermediate ensemble. Studies of the variant YY show properties akin to those of L53AI54A, trapping a hyperfluorescent partially folded species as the ground state of the folding reaction that resembles closely the intermediate populated transiently during folding of wild-type Im7\* (Figure 1B) (G. R. Spence and S. E. Radford, unpublished data).

The UVRR spectrum of wild-type Im7\* and the variant L53AI54A are compared in spectra A and B of Figure 5. Positive features are observed in the L53AI54A minus Im7\* difference spectrum for the W18, W17, W16, W7, and W3 bands (Figure 5C), indicating that all of the bands arising from tryptophan are enhanced in intensity in the spectrum of the variant protein. The UVRR band intensity of tryptophan residues is known to be sensitive to the strength of hydrogen bonding to the indole nitrogen as well as to the hydrophobicity of the local environment of the indole ring (33, 34). The W17 band position occurs at the same wavenumber (879 cm<sup>-1</sup>) in both wild-type Im7\* and L53AI54A, indicating that there is no difference in the hydrogen bonding state of the indole ring of Trp75 in both proteins. Thus, the general increase in tryptophan band intensity in L53AI54A can be attributed to an increase in the overall hydrophobicity of the environment of Trp75 in this variant. Time-resolved measurements of the fluorescence decay of Trp75 and fluorescence quenching experiments (13) on Im7\* and its variant proteins performed to assess the accessibility of Trp75 to solvent yielded a mean lifetime of  $1.98 \pm 0.068$  ns and a quenching constant ( $k_q$ ) of  $(0.75 \pm 0.027) \times 10^9$  M<sup>-1</sup> s<sup>-1</sup> for Im7\*, whereas L53AI54A presents a mean lifetime of  $5.15 \pm 0.1$  ns and a  $k_q$  of  $(0.54 \pm 0.022) \times 10^9$  M<sup>-1</sup> s<sup>-1</sup> (Table 3). The increase in fluorescence lifetime and the reduction in the  $k_q$  value in L53AI54A relative to that of Im7\* suggest that the accessibility of Trp75 to the solvent is reduced in L53AI54A compared with Im7\*. These data are consistent with the results from fluorescence emission spectroscopy, which show

a large increase in tryptophan fluorescence intensity of the variant protein relative to that of wild-type Im7\* [Figure 1B (13)], presumably because the tryptophan is buried from solvent, but is not yet juxtaposed with His47, which quenches the fluorescence of Trp75 in the native state of the wild-type protein (8, 13). Moreover, the peak emission wavelength of Trp75 in the variant L53AI54A is 334 nm (13), consistent with burial of the tryptophan from the solvent. The fluorescence of Trp75 in the native state of wild-type Im7\* is almost totally quenched by a ring stacking interaction with His47; thus, the change in the  $\lambda_{max}$  of tryptophan fluorescence between wild-type Im7\* and the variant L53AI54A cannot be determined. The UVRR spectra and the time-resolved fluorescence measurements presented provide important new information about the unusual hyperfluorescence of this Im7\* folding intermediate, suggesting that the environment local to Trp75 is more hydrophobic in the variant than in the wild-type protein.

Insights into the nature of the environment involving the three tyrosine residues in the variant L53AI54A were also obtained by analysis of the Y9a, Y7a, and Y8a/b bands using UVRR excited at 229 nm. The L53AI54A minus Im7\* difference spectrum (Figure 5C) indicates a decrease in the intensity of these bands in L53AI54A compared with those in wild-type Im7\*. Deconvolution of the overlapped Y8a and Y8b modes shows Y8a at 1616.1 cm<sup>-1</sup> and Y8b at 1600.7 cm<sup>-1</sup> in L53AI54A, frequencies very similar to those observed for these bands in wild-type Im7\*, indicating that there is little or no change in the average hydrogen bonding state of these residues (see Figure S1 of the Supporting Information and Table 2). The Raman excitation profiles of tyrosine bands are red-shifted when a phenolic OH group is hydrogen bonded to an acceptor residue, as well as by an increased environmental hydrophobicity (31). The overall decrease in intensity of all tyrosine bands observed in L53AI54A relative to Im7\* suggests, therefore, that there is an overall decrease in hydrophobicity of one or more of the tyrosine residues in this variant.

As with L53AI54A, the H3G6 mutant also traps a partially folded state of Im7\* at equilibrium, although by contrast with L53AI54A, this species is not hyperfluorescent (Figure 1B) (13). The UVRR H3G6 minus Im7\* difference spectrum (Figure 5E) shows positive peaks for all tryptophan bands, while the W17 band remains at 879 cm<sup>-1</sup> in both proteins. Together, these data indicate that the enhancement of the band intensities resulting from tryptophan residues in H3G6 reflects an increase in the hydrophobicity of the environment local to Trp75 in this variant. H3G6 presents a mean fluorescence lifetime of  $4.81 \pm 0.1$  ns compared with  $1.98 \pm 0.068$  ns in the case of Im7\*, which is in agreement with

the increase in fluorescence intensity observed in this variant, possibly resulting from a reduction in the degree of solvent quenching. The fluorescence emission  $\lambda_{\text{max}}$  of H3G6 occurs at 340 nm. This peak is red-shifted relative to that of L53AI54A, consistent with only partial burial of Trp75 in H3G6. Additionally, H3G6 presents differences in the near-UV CD spectrum relative to that of L53AI54A, which is evidence of changes in the arrangement of aromatic side chains (13). Furthermore, the positive peaks in the L53AI54A minus Im7\* difference spectrum (Figure 5C) are increased in intensity relative to those of the H3G6 minus Im7\* difference spectrum (Figure 5E), revealing an enhancement in the intensity of the tryptophan Raman bands in L53AI54A relative to H3G6. In agreement with this, the variant H3G6 has a measured Stern–Volmer constant ( $K_{\text{sv}}$ ) of  $4.0 \text{ M}^{-1}$  (13) and a calculated  $k_{\text{q}}$  of  $(0.83 \pm 0.044) \times 10^9 \text{ M}^{-1} \text{ s}^{-1}$ , a value significantly larger than that for L53AI54A and close to that calculated for Im7\* (Table 3). The fluorescence results thus suggest that the solvent accessibility of the tryptophan side chain in the variant H3G6 is increased relative to that of L53AI54A and is similar to that of wild-type Im7\*. The UVRR data indicate, however, that the environment local to Trp75 must differ in the variant protein and Im7\* to account for the overall increase in hydrophobicity in the environment of Trp75 in H3G6 detected using this technique. Major spectral changes in the bands arising from tyrosine residues in the difference spectrum between Im7\* and H3G6 simply reflect the fact that two tyrosine residues (Tyr55 and Tyr56; Figure 1A, inset) have been deleted in this variant. The tyrosine bands observed for the variant H3G6, therefore, can be attributed to the single tyrosine (Tyr10) in the N-terminal region of this protein.

In terms of its fluorescence properties, the variant YY is similar to L53AI54A in that both proteins are hyperfluorescent (Figure 1B). The maximum emission wavelength of YY (337 nm) and tryptophan solvent accessibility measured using iodide quenching experiments for the variants YY and L53AI54A [ $K_{\text{sv}} = 2.9$  and  $2.8 \text{ M}^{-1}$  (13), respectively] are also similar (Table 3). This similarity is also borne out by the UVRR data for YY (Figure 5F,G, and Figure S2 of the Supporting Information). In the YY minus Im7\* difference spectrum (Figure 5G), positive features for tryptophan bands W18, W17, W16, W7, and W3 are observed, indicative of an increase in the environmental hydrophobicity of Trp75 in this variant (as observed for the other variants there is no shift in the W17 band position in YY compared with wild-type Im7\*, ruling out changes in hydrogen bonding as the origin of the intensity differences). The mean fluorescence lifetime and  $k_{\text{q}}$  values for YY [ $5.05 \pm 0.1 \text{ ns}$  and  $(0.585 \pm 0.022) \times 10^9 \text{ M}^{-1} \text{ s}^{-1}$ , respectively] are identical to those for L53AI54A (Table 3), indicating a common decrease in the accessibility of Trp75 to the solvent in both variants relative to wild-type Im7\*. The UVRR YY minus L53AI54A difference spectrum is also featureless in intensity at the band positions arising from tryptophan residues (see Figure S2 of the Supporting Information), indicating that the hydrophobicity of the environment local to Trp75 is identical in these proteins. While there are no features in the difference spectra between YY and Im7\* (Figure 5G) at band positions Y9a and Y7a, a derivative feature is observed in the 1610–1614  $\text{cm}^{-1}$  region, suggesting a small change in frequency of bands Y8a and Y8b, respectively, in the spectrum of YY (see Figure

S1 of the Supporting Information and Table 2) (the positive peak in the difference spectrum at  $1621 \text{ cm}^{-1}$  is assigned to an increase in the intensity of the tryptophan W1 band in YY relative to Im7\*). Since there is no obvious general decrease in the band intensities of tyrosine residues in YY with respect to Im7\*, the small frequency shifts of the Y8a and Y8b modes could suggest subtle changes in the hydrogen bonding state of Tyr55 and/or Tyr56 in this variant, without direct evidence of a net loss of hydrogen bonding or significant changes in the hydrophobicity associated with the tyrosine residues. Perhaps more significantly, however, the YY minus L53AI54A difference spectrum shows clear features arising from tyrosine residues, suggesting that despite the similar environment of Trp75 in these proteins, the environment local to one or more tyrosine residues differs significantly (Figure S2 of the Supporting Information).

## DISCUSSION

Here we have presented a detailed analysis of the conformational properties of the tryptophan and tyrosine residues in wild-type Im7\* and Im9\* measured using UVRR excited at 229 nm, together with a description of the environment of these residues in three variants of Im7\* designed to trap a partially folded state at equilibrium. The data show that the UVRR spectra of wild-type Im7\* and Im9\* are identical, indicating that the tryptophan and tyrosine residues in the two proteins adopt conformations that cannot be distinguished by UVRR. Interestingly, the W17 band position in these proteins, together with the X-ray and NMR structures of these proteins (1, 17), indicates that Trp75 is partially exposed and involved in hydrogen bonding with solvent in both proteins. However, the tryptophan Fermi doublet ratio ( $I_{1360}/I_{1340}$ ) at 229 nm suggested a relatively hydrophobic environment for this side chain. A brief study of the wavelength dependence of the tryptophan Fermi doublet ratio using both model compounds and the series of immunity proteins studied here revealed an important and unexpected dependence of this ratio on the excitation wavelength, questioning the validity of the simple interpretation of this feature under resonance conditions based on model compound studies using visible radiation (24). Regardless of possible uncertainties in the interpretation of the Fermi doublet, the Im7\* minus Im9\* difference spectrum is featureless, demonstrating that the environment local to tryptophan and tyrosine residues in these proteins, together with their hydrogen bonding properties, is identical. Interestingly, and by contrast with these data, the X-ray crystal and NMR solution structures of Im7 and Im9, respectively (1, 17), show rather different properties of the single tryptophan residue, specifically in its  $\chi^{2,1}$  angle and in its exposure to solvent. These differences may reflect unusual compensating effects in the environments of the aromatic rings in these proteins that cancel out the expected differences in their UVRR spectra, or from differences in the solution properties of Im7 compared with its crystalline form. However, what is clear is that both the electron density in the X-ray crystal structure (1) and the number of constraints in the NMR solution structure (17) rule out errors in the structure determination as one possible cause.

The UVRR data presented above cast new light on the structural properties of the partially folded states of Im7\*, particularly in the environment of the single tryptophan

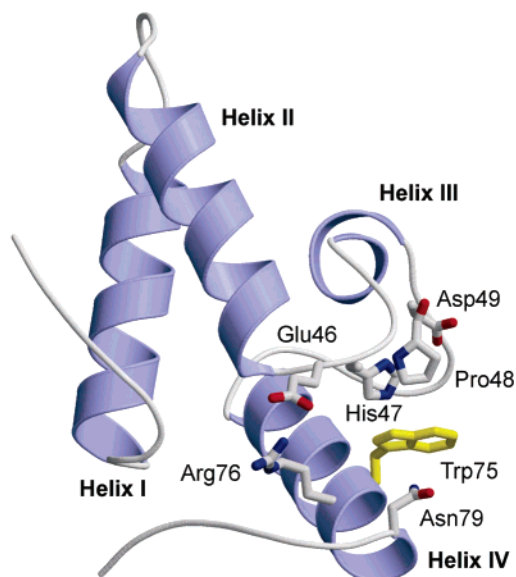


FIGURE 6: Ribbon diagram showing the pocket containing Trp75 in wild-type Im7. The side chains that are shown include those that make significant contacts with the side chain of Trp75. This figure was drawn using Molscript (36) and Raster3D (37) from the coordinates of the crystal structure of Im7 (PDB entry 1AYI) (1).

residue that gives rise to the unusual fluorescence properties of these species. The UVRR data clearly indicate that the underlying structural changes induced by the mutations in the Im7\* variants, L53AI54A, H3G6, and YY, result in an increase in the hydrophobicity of the environment local to Trp75 compared with wild-type Im7\*. The increase in fluorescence emission intensity reported for these variants compared with the native state of wild-type Im7\* (13) is consistent with these data. Our current time-resolved fluorescence measurements together with previous fluorescence quenching data (13) indicate a decrease in the overall solvent accessibility of Trp75 in the variants L53AI54A and YY, while the accessibility of Trp75 in the variant H3G6 remains close to that of wild-type Im7\*. UVRR is known to be a sensitive probe of the solvent accessible surface area of tyrosine and tryptophan residues in proteins; the smaller the area exposed, the greater the Raman band intensities are expected to be (30, 33, 34). The UVRR data indicate an increased hydrophobicity local to the indole ring in all of these variants. In the native state of wild-type Im7, Trp75 is located in a pocket situated at one edge of the protein structure, the indole ring of Trp75 making contact (within 6 Å) with one or more atoms in Thr45, Glu46, His47, Pro48, Glu71, Ile72, Glu74, Arg76, Ala78, and Asn79 (Figure 6). The indole ring also is partially solvent exposed [105 Å<sup>2</sup>, which equates to 52% of the total surface area of an indole ring (35)]. Of the residues that make contact with Trp75, all but Pro48, Ile72, and Ala78 are hydrophilic in character. The hydrophilic side chains of Glu46, His47, Arg76, and Asn79 are predominantly responsible for creating the pocket within which the indole ring of Trp75 is confined (Figure 6) (1). We suggest that the reported increase in the UVRR band intensity of Trp75 in the variants L53AI54A, YY, and H3G6 relative to wild-type Im7\* arises from the withdrawal of the hydrophilic contribution of Glu46 and/or His47 from the environment of Trp75 by the displacement of the loop (Glu46–Gly50) that joins helices II and III and forms part

of the Trp75 pocket in Im7, although other conformational rearrangements involving larger movements from the native structure cannot be ruled out. The reorganization of the tryptophan pocket must also account for the decrease in accessibility of Trp75 to solvent in the variants L53AI54A and YY, which will additionally contribute to the increase in the Raman band intensity of Trp75 in the hyperfluorescent variants. The displacement of this loop may then result in the increased fluorescence intensity of the variants relative to wild-type Im7\*, by the formation of new interactions between Trp75 and residues more hydrophobic in character. For H3G6, by contrast, little change in the solvent accessible surface area of Trp75 relative to that of wild-type Im7\* occurs. Nonetheless, the UVRR data presented here demonstrate that changes local to Trp75 must occur such that the relative hydrophobicity of the environment involving this residue is increased, resulting in an increase in the fluorescence lifetime of Trp75 relative to that of wild-type Im7\*. The UVRR studies presented here, therefore, indicate that a newly formed hydrophobic environment is a shared property of all of the variants of Im7\* studied and reveal that subtle changes local to the environment of these residues can lead to significant changes in their fluorescence properties. These data substantiate the results of  $\phi$ -value analysis (6) by providing direct evidence that the environment local to Trp75 in partially folded Im7\* is both non-native and hydrophobic in nature.

#### ACKNOWLEDGMENT

We thank Claire Friel for Im9\* protein, members of the Smith and Radford groups for helpful discussions, and David Batchelder for many informative discussions.

#### SUPPORTING INFORMATION AVAILABLE

Position of the Y8b and Y8a modes for Im7\* and the three variants obtained by curve fitting the 1510–1680 cm<sup>-1</sup> region with 50% Gaussian and 50% Lorentzian bands, UVRR spectra of YY and L53AI54A, and the YY minus L53AI54A difference spectrum excited at 229 nm. This material is available free of charge via the Internet at <http://pubs.acs.org>.

#### REFERENCES

- Dennis, C. A., Videler, H., Pauptit, R. A., Wallis, R., James, R., Moore, G. R., and Kleanthous, C. (1998) A structural comparison of the colicin immunity proteins Im7 and Im9 gives new insights into the molecular determinants of immunity-protein specificity, *Biochem. J.* 333, 183–191.
- Kleanthous, C., and Walker, D. (2001) Immunity proteins: Enzyme inhibitors that avoid the active site, *Trends Biochem. Sci.* 26, 624–631.
- Friel, C. T., Beddard, G. S., and Radford, S. E. (2004) Switching two-state to three-state kinetics in the helical protein Im9 via the optimisation of stabilising non-native interactions by design, *J. Mol. Biol.* 342, 261–273.
- Ferguson, N., Capaldi, A. P., James, R., Kleanthous, C., and Radford, S. E. (1999) Rapid folding with and without populated intermediates in the homologous four-helix proteins Im7 and Im9, *J. Mol. Biol.* 286, 1597–1608.
- Gorski, S. A., Capaldi, A. P., Kleanthous, C., and Radford, S. E. (2001) Acidic conditions stabilise intermediates populated during the folding of Im7 and Im9, *J. Mol. Biol.* 312, 849–863.
- Capaldi, A. P., Kleanthous, C., and Radford, S. E. (2002) Im7 folding mechanism: Misfolding on a path to the native state, *Nat. Struct. Biol.* 9, 209–216.

7. Friel, C. T., Capaldi, A. P., and Radford, S. E. (2003) Structural analysis of the rate-limiting transition states in the folding of Im7 and Im9: Similarities and differences in the folding of homologous proteins, *J. Mol. Biol.* *326*, 293–305.
8. Wallis, R., Leung, K.-Y., Osborne, M. J., James, R., Moore, G. R., and Kleanthous, C. (1998) Specificity in protein–protein recognition: Conserved Im9 residues are the major determinants of stability in the colicin E9 DNase-Im9 complex, *Biochemistry* *37*, 476–485.
9. Li, W., Keeble, A. H., Giffard, C., James, R., Moore, G. R., and Kleanthous, C. (2004) Highly discriminating protein–protein interaction specificities in the context of a conserved binding energy hotspot, *J. Mol. Biol.* *377*, 743–759.
10. Asher, S. A., Bormett, R. W., Chen, X. G., Lemmon, D. H., Cho, N., Peterson, P., Arrigoni, M., Spinelli, L., and Cannon, J. (1993) UV resonance Raman spectroscopy using a new cw laser source: Convenience and experimental simplicity, *Appl. Spectrosc.* *47*, 628–633.
11. Harada, I., and Takeuchi, H. (1986) Raman and ultraviolet resonance Raman spectra of proteins and related compounds, in *Spectroscopy of Biological Samples* (Clark, R. J. H., and Hester, R. H., Eds.) pp 113–175, Wiley, New York.
12. Austin, J. C., Jordan, T., and Spiro, T. G. (1993) Ultraviolet resonance Raman studies of proteins and related model compounds, *Adv. Spectrosc.* *20*, 55–127.
13. Spence, G. R., Capaldi, A. P., and Radford, S. E. (2004) Trapping the on-pathway folding intermediate of Im7 at equilibrium, *J. Mol. Biol.* *341*, 215–226.
14. Gill, S. C., and von Hippel, P. H. (1989) Calculation of protein extinction coefficients from amino acid sequence data, *Anal. Biochem.* *182*, 319–326.
15. Sands, H. S., Demangeot, F., Bonera, E., Webster, S., Bennett, R., Hayward, I. P., Marchi, F., Smith, D. A., and Batchelder, D. N. (2002) Development of a combined confocal and scanning near-field Raman microscope for deep UV laser excitation, *J. Raman Spectrosc.* *33*, 730–739.
16. Wallis, R., Reilly, A., Rowe, A. J., Moore, G. R., James, R., and Kleanthous, C. (1992) *In vivo* and *in vitro* characterization of overproduced colicin E9 immunity protein, *Eur. J. Biochem.* *207*, 687–695.
17. Osborne, M. J., Breeze, A. L., Lian, L.-Y., Reilly, A., James, R., Kleanthous, C., and Moore, G. R. (1996) Three-dimensional solution structure and <sup>13</sup>C nuclear magnetic resonance assignments of the colicin E9 immunity protein Im9, *Biochemistry* *35*, 9505–9512.
18. Sweeney, J. A., and Asher, S. A. (1990) Tryptophan UV resonance Raman excitation profiles, *J. Phys. Chem.* *94*, 4784–4791.
19. Asher, S. A., Ludwig, M., and Johnson, C. R. (1986) UV resonance Raman excitation profiles of the aromatic amino acids, *J. Am. Chem. Soc.* *108*, 3186–3197.
20. Ludwig, M., and Asher, S. A. (1988) Ultraviolet resonance Raman excitation profiles of tyrosine: Dependence of Raman cross sections on excited-state intermediates, *J. Am. Chem. Soc.* *110*, 1005–1011.
21. Rava, R. P., and Spiro, T. G. (1985) Resonance enhancement in the ultraviolet Raman spectra of aromatic amino acids, *J. Phys. Chem.* *89*, 1856–1861.
22. Miura, T., Takeuchi, H., and Harada, I. (1988) Characterization of individual tryptophan side chains in proteins using Raman spectroscopy and hydrogen–deuterium exchange kinetics, *Biochemistry* *27*, 88–94.
23. Sobolev, V., Sorokine, A., Prilusky, J., Abola, E. E., and Edelman, M. (1999) Automated analysis of interatomic contacts in proteins, *Bioinformatics* *15*, 327–332.
24. Harada, I., Miura, T., and Takeuchi, H. (1986) Origin of the doublet at 1360 and 1340 cm<sup>-1</sup> in the Raman spectra of tryptophan and related compounds, *Spectrochim. Acta* *42A*, 307–312.
25. Takeuchi, H., and Harada, I. (1986) Normal coordinate analysis of the indole ring, *Spectrochim. Acta* *42A*, 1069–1078.
26. McHale, J. L. (1982) Fermi resonance of tyrosine and related compounds. Analysis of the Raman doublet, *J. Raman Spectrosc.* *13*, 21–24.
27. Miura, T., Takeuchi, H., and Harada, I. (1989) Tryptophan Raman bands sensitive to hydrogen bonding and side-chain conformation, *J. Raman Spectrosc.* *20*, 667–671.
28. Maruyama, T., and Takeuchi, H. (1995) Effects of hydrogen bonding and side-chain conformation on the Raman bands of tryptophan-2,4,5,6,7-*d*<sub>5</sub>, *J. Raman Spectrosc.* *26*, 319–324.
29. Hildebrandt, P. G., Copeland, R. A., Spiro, T. G., Otlewski, J., Laskowski, M., and Prendergast, F. G. (1988) Tyrosine hydrogen-bonding and environmental effects in proteins probed by ultraviolet resonance Raman spectroscopy, *Biochemistry* *27*, 5426–5433.
30. Chi, Z., and Asher, S. A. (1998) UV Raman determination of the environment and solvent exposure of Tyr and Trp residues, *J. Phys. Chem. B* *102*, 9595–9602.
31. Rodgers, K. R., Su, C., Subramanian, S., and Spiro, T. G. (1992) Hemoglobin R–T structural dynamics from simultaneous monitoring of tyrosine and tryptophan time-resolved UV resonance Raman signals, *J. Am. Chem. Soc.* *114*, 3697–3709.
32. Takeuchi, H., Watanabe, N., Satoh, Y., and Harada, I. (1989) Effects of hydrogen bonding on the tyrosine Raman bands in the 1300–1150 cm<sup>-1</sup> region, *J. Raman Spectrosc.* *20*, 233–237.
33. Chi, Z., and Asher, S. A. (1998) UV Raman determination of protein acid denaturation: Selective unfolding of helical segments of horse myoglobin, *Biochemistry* *37*, 2865–2872.
34. Matsuno, M., and Takeuchi, H. (1998) Effects of hydrogen bonding and hydrophobic interactions on the ultraviolet resonance Raman intensities of indole ring vibrations, *Bull. Chem. Soc. Jpn.* *71*, 851–857.
35. Karplus, P. A. (1997) Hydrophobicity regained, *Protein Sci.* *6*, 1302–1307.
36. Kraulis, P. J. (1991) MOLSCRIPT: A program to produce both detailed and schematic plots of protein structures, *J. Appl. Crystallogr.* *24*, 946–950.
37. Merrit, E. A., and Bacon, D. J. (1997) Raster3D: Photorealistic molecular graphics, *Methods Enzymol.* *277*, 505–524.

BI047746K